Thermodynamics, kinetics, and mechanics of cesium sorption in cement paste: A multiscale assessment

Jack Arayro,[1,2] Alice Dufresne,[3] Tingtao Zhou,[4] Katerina Ioannidou,[1,3] Josef-Franz Ulm,[3] Roland Pellenq,[1,3,5] and Laurent Karim Béland[1,6,*]

[1]*MultiScale Materials Science for Energy and Environment (MSE2), The Joint CNRS/MIT/Aix-Marseille University Laboratory, UMI CNRS 3466, Massachusetts Institute of Technology, Cambridge, MIT 02139, Massachusetts, USA*

[2]*College of Engineering and Technology, American University of the Middle East, Eqaila 54200, Kuwait*

[3]*Department of Civil and Environmental Engineering, Massachusetts Institute of Technology, Cambridge, Queen's K7L 3N6, Massachusetts, USA*

[4]*Department of Physics, Massachusetts Institute of Technology, Cambridge, Massachusetts, USA*

[5]*CINaM-Aix Marseille Université-CNRS, Marseille, France*

[6]*Department of Mechanical and Materials Engineering, Queen's University, Kingston, Ontario, Canada*

(Received 6 December 2017; published 30 May 2018; corrected 18 August 2023)

Cesium-137 is a common radioactive byproduct found in nuclear spent fuel. Given its 30 year half life, its interactions with potential storage materials—such as cement paste—is of crucial importance. In this paper, simulations are used to establish the interaction of calcium silicate hydrates (C-S-H)—the main binding phase of cement paste—with Cs at the nano- and mesoscale. Different C-S-H compositions are explored, including a range of Ca/Si ratios from 1.0 to 2.0. These calculations are based on a set of 150 atomistic models, which qualitatively and quantitatively reproduce a number of experimentally measured features of C-S-H—within limits intrinsic to the approximations imposed by classical molecular dynamics and the steps followed when building the models. A procedure where hydrated Ca^{2+} ions are swapped for Cs^{1+} ions shows that Cs adsorption in the C-S-H interlayer is preferred to Cs adsorption at the nanopore surface when Cs concentrations are lower than 0.19 Mol/kg. Interlayer sorption decreases as the Ca/Si ratio increases. The activation relaxation technique *nouveau* is used to access timescales out of the reach of traditional molecular dynamics (MD). It indicates that characteristic diffusion time for Cs^{1+} in the C-S-H interlayer is on the order of a few hours. Cs uptake in the interlayer has little impact on the elastic response of C-S-H. It leads to swelling of the C-S-H grains, but mesoscale calculations that access length scales out of the range of MD indicate that this leads to practically negligible expansive pressures for Cs concentrations relevant to nuclear waste repositories.

DOI: 10.1103/PhysRevMaterials.2.053608

I. INTRODUCTION

Stanley Kubrick's Dr. Strangelove—portayed by Peter Sellers—created an array of cobalt jacketed atomic bombs. Cobalt bombs are intended to contaminate the environment on a large scale with long-lasting radioactive materials, namely Cs-137. It is abundantly found in spent fuel and in exchange resins used to purify coolant water in nuclear power plants [1]. It is highly soluble, chemically reactive [2], and it has an intermediate half life of 30.17 years [3] along with a high radioactivity of 3.2×10^{12} Bq/g [3–5]. It can penetrate into the soil and enter the food chain [6], making this element dangerous to human health. Thus, Cs-137 should be confined.

In this context, concrete and its binder—cement paste—are leading candidates as storage materials for low- and mid-level nuclear waste. Also, as some of the main structural materials used for the construction of nuclear power plants, their ability to sorb or contain Cs is of technological interest, notably in reactor leakage and decommissioning scenarios. As a consequence, a number of experiments were conducted to understand the behavior of Cs in cement paste. We refer the reader to a review by Evans [7] about the binding mechanisms of radionuclides to cement. There is a consensus that C-S-H is the main phase responsible for Cs binding [8–11] and that the main sorption process of Cs in CSH is ion exchange [11–13]. We note that the effect of the Ca/Si ratio of the C-S-H on the Cs retention is the subject of debate in the literature—most studies found that Cs retention decreases with an increase of the Ca/Si ratio [7,11,14,15], but one study found the opposite [16]. Iwaida *et al.* [9] suggest that Cs fragments the tobemorite-type layer. Tobermorite is a C-S-H mineral, with a Ca/Si ratio of 0.83, which is composed of oxide planes separated by hydrated interlayers, thought to resemble the oxide layers of C-S-H in cement paste. They also observe expansion of the basal plane distance after sorption of Cs. In regards to mechanical properties, Hoyle and Grutzeck [17] showed that compressive strength is changed by the addition of Cs, but in a nonsystematic way. In regard to kinetics, Cs sorption time is roughly one day [15,18].

There are also a number of computational studies of Cs. We also note reports involving lighter alkali elements—K and Na—as their behavior in C-S-H is—to some extent—analogous to that of Cs. Dezerald *et al.* [19] studied the ability of C-S-H to contain nuclear waste: C-S-H was mechanically stable upon insertion of Sr-90 and its daughter nucleus, Y-90

*laurent.beland@queensu.ca

and Zr-90. Ruiz Pestana *et al.* [20] calculated ion diffusion barriers in nonswelling clays—namely Illite, a more ordered system than C-S-H. They found activation barriers of the order of 50 kCal/mol for K^+ and Cs^+ diffusion in C-S-H. Ozccelik and White [21] found similarly large barriers (approx. 30 kCal/mol) for Na^+ diffusion in tobermerite, which is expected to have a smaller diffusion barrier than Cs^+, because of its small ionic radius. Also, they find that hydrated Ca^{2+} are more likely to be exchanged for alkali ions than intralayer Ca or Si. Finally, Jiang *et al.* [22] recently reported MD simulations of Cs ions binding to a tobermorite nanopore surface. They observe exchange of Ca^{2+} for Cs^+. However, they did not assess sorption in the hydrated interlayer, nor have they estimated the effect of adsorption on the mechanical properties of cement paste.

In this paper, multiscale calculations—both length and time scales—of the thermodynamics, kinetics, and mechanical effects of Cs sorption in C-S-H are reported. The thermodynamics are computed using a semigrand canonical framework. The kinetics are calculated using transition-state theory, a long timescale framework. The mechanical properties of the Cs-containing C-S-H are calculated by a mix of nanoscale and mesoscale calculations. We conclude the paper with a short discussion and conclusions.

II. METHODOLOGY

A. Interaction force field

Force and energies are calculated using the CSHFF [23] potential, adapted for alkali ions. CSHFF [23] is itself based on ClayFF [24]. This potential has a Coulombic part, Van der Waals interactions, as well as harmonic bonds for hydroxyl groups and harmonic angular springs for water. The C-S-H and nanopore models built with this potential have been thoroughly validated against experiments [25,26]. All the parameters for the CSHFF are as described in Ref. [23]. The original ClayFF does have a parametrization for Cs^{1+}, but CSHFF does not. The former is introduced into the latter. A partial charge of 0.852765 e^- is given to the Cs ion, to be consistent with the rest of the CSHFF model. The Van der Waals equilibrium distance parameters $R_{0,ij}$ between the Cs ions and the surrounding atoms are determined by arithmetic averaging. The validity of this parametrization of alkali interactions in CSHFF was successfully benchmarked against the equilibrium volume and atomic positions in the unit cell of three alkali-rich mineral structures: combeite [27], hydroxyapophyllite [28], and senkevichite [29]. More details of this validation can be found in the Supplemental Material [30].

The MD calculations in this study are performed using the LAMMPS package [31], with a timestep of 1 fs for NVT and NPT simulations. The Nose-Hoover thermostat is used.

B. Nanoscale C-S-H models

The C-S-H models from Ref. [26] are used. There are 150 such atomistic models, each containing about 500 atoms, with Ca/Si ratio varying from 1 to 2. A model is illustrated in the right panel of Fig. 1. They have been shown to reproduce diffraction, nuclear magnetic resonance (NMR), water uptake, silica chain length, thermal conductivity, and mechanical measurements [26,32–34]. These models were built using the following procedure:

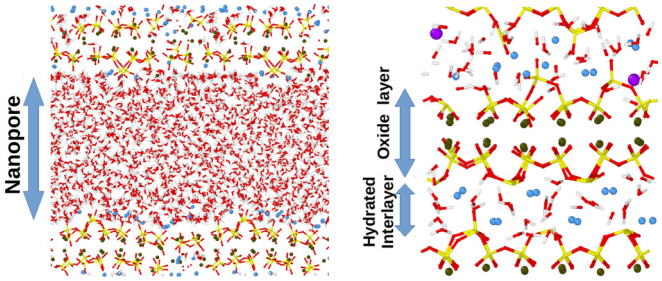

FIG. 1. Left panel: a snapshot of the nanopore model. Right panel: a snapshot of the C-S-H interlayer model. Silicon are yellow, hydrated Ca^{2+} are blue, intralayer Ca^{2+} are green, hydrogen are white, oxygen are red, and Cs^+ is purple. The nanopore, interlayer, and oxide layers are identified.

(1) Start with tobermorite 11 Å.
(2) Remove all water.
(3) Remove random SiO_2.
(4) Adsorb water at 1 bar using GCMC (CSHFF).
(5) React using reactive MD (ReaxFF).
(6) Proceed to simulated annealing (CSHFF).

There are other proposals as to the atomistic structure of C-S-H. For instance, Kumar *et al.* [35] proposed a structure based on tobermorite 14 Åthat systematically introduced well defined defects, namely removing SiO_2 bridging sites, via a Monte Carlo procedure. It turns a so-called $Q^{(2b)}$ site into a $Q^{(1)}$ site, which in turns requires introduction of H^+ and $CaOH^+$ to locally conserve charge. They also allow for introduction of H_2O and $Ca(OH)_2$. The defect is considered adequate if experimental atomic bond distances, coordination numbers, and local charge balance are reproduced after a DFT structural relaxation. The Monte Carlo procedure is repeated until the distribution of silica chain length satisfies ratios based on the experimentally observed proportions of $Q^{(2b)}$ and $Q^{(1)}$. The outcome is a structure that closely reproduces the NMR data, with no glassy behavior even at Ca/Si ratio > 1.5. One should note that their Monte Carlo method and analysis of the NMR data explicitly exclude the presence of silica monomers ($Q^{(0)}$).

Another recent proposal was made by Kovačević *et al.* [36,37]. Their scheme is also based on modifying tobermorite, removing SiO_2 from bridging silicate sites and adding Ca ions to the interlayer. Water is introduced randomly—given geometrical constraints—in order to obtain a target H/Si ratio. Charge is then balanced by removing H ions from water near Ca ions. The ReaxFF and PM6 force fields are then used to react the system and relax it. This procedure led to energetically favorable results, compared to procedures where silica were removed from random sites or where no $CaOH^+$ was added to the interlayer.

One important point of debate is the presence of silica monomers ($Q^{(0)}$) in the Qomi *et al.* [26] models. One factor of this debate was that NMR measurements were inconclusive. However, a recent high-resolution NMR study [38] quantified the $Q^{(0)}$ fraction at 5%. This is in good agreement with the Qomi models, that predicts a value of 6%, if averaged over the experimental Ca/Si ratio distribution. Another point raised by Kovačević *et al.* [36,37] is that selecting random SiO_2 sites for deletion led to C-S-H systems with a higher energy than

those where bridging SiO_2 sites were chosen. However, their procedure is different from that of Qomi *et al.* in three ways. First, water is introduced through GCMC by Qomi *et al.*, while it is introduced geometrically by Kovačević *et al.*. Second, Qomi *et al.* used the CSH-FF potential, while Kovačević *et al.* used PM6. Third, Qomi *et al.* performed a simulated anneal of the configurations, which was not performed by Kovačević *et al.* A last point to highlight is that the Ca-Si layers in C-S-H with a high Ca/Si ratio tend to be deprotonated [39], which in turn leads to increase in $CaOH^+$ content in the interlayer. The procedure employed by Qomi *et al.* does not guarantee this deprotonation of the Ca-Si layer, although it does predict the correct number of Ca-OH bonds per Si atom. Nonetheless, the models by Qomi *et al.* [26] were extensively validated against experiments, as mentioned above, to a far greater extent than any other model, to the best of our knowledge. For this reason, they were chosen as a basis for this study.

It should be emphasized that the choice of force field has an impact on the physical accuracy of our calculations that is likely comparable to—or larger than—the details of the model's nanostructure. Nonetheless, the models by Qomi *et al.* [26] were extensively validated against experiments to a far greater extent than any other model, to the best of our knowledge. For this reason, they were chosen as a basis for this study.

C. Semigrand canonical Monte Carlo

Sorption of Cs^+ in the C-S-H interlayer was simulated. An ion exchange mechanism similar to that found in clay minerals is assumed—i.e., maintaining ionic charges content throughout the process. In all calculations, each addition of two Cs^{1+} is balanced by removing one Ca^{2+}. Our tests showed that hydrated Ca^{2+} sites are energetically preferable to the removal of Ca^{2+} intralayer ions, in agreement with Ref. [21].

Exchange of ions in the interlayer is considered by a semigrand canonical approach. The procedure is reminiscent of Ref. [40]. In that reference, however, the ions swapped have the same charge and can be swapped one-for-one. In the case of Cs, each hydrated Ca ion is swapped for two Cs ions. Concentrations between [0,5.8] Mol/kg were considered in the interlayer, i.e., exchanging none to all the hydrated Ca^{2+} ions. The nanopore surface was considered as a sink and source of ions. The chemical potential difference can be estimated as the average binding energies of surface Ca^{2+} and Cs^+ ions in a nanopore model. The model described in Ref. [25] is used. This is a 2.483 nm C-S-H configuration containing a gel pore at 100% humidity.

In addition to the assumption that no charge transfer takes place, it was also assumed that the potential energy minima explain the thermodynamics of sorption. This assumption was validated by comparing results solely based on potential energy minima to approaches involving MD-based configuration sampling.

Here is the Monte Carlo procedure that was chosen for exchange in the C-S-H interlayer. Cs corresponds to Cs ions, while Cw corresponds to hydrated Ca ions:

(1) The system is minimized to a local potential energy minimum E_{before}.

(2) One of three moves is made:

(a) 40% of the moves: If at least one Cs and one Cw are present, the positions of a Cs and a Cw are exchanged.

(b) 30% of the moves: If at least two Cs are present, replace a Cs by a Cw and delete another Cs.

(c) 30% of the moves: If at least one Cw is present, replace a Cw by a Cs and add a Cs in a random position.

(3) The system is minimized to a local potential energy minimum E_{after}. $\Delta E = E_{\text{after}} - E_{\text{before}}$

(4) Accept or reject the move. Respectively:

(a) Use the standard Metropolis acceptance criteria.

(b) Accept with probability $P_{2Cs\rightarrow Cw}$.

(c) Accept with probability $P_{Cw\rightarrow 2Cs}$.

The probabilities for the swaps are as follows:

$$P_{Cw\rightarrow 2Cs} = \left(\frac{2\pi\beta}{h^2}\frac{m_{Cs}^2}{m_{Cw}}\right)^{3/2} \times \frac{V N_{Cw}}{(N_{Cs}+1)(N_{Cs}+2)} e^{-\beta(\Delta E - \Delta'\mu)} \quad (1)$$

$$P_{2Cs\rightarrow Cw} = \left(\frac{2\pi\beta}{h^2}\frac{m_{Cs}^2}{m_{Cw}}\right)^{-3/2} \times \frac{N_{Cs}(N_{Cs}-1)}{V(N_{Cw}+1)} e^{-\beta(\Delta E + \Delta'\mu)} \quad (2)$$

with N_{Cw} and N_{Cs} the initials atom number of Cw and Cs, $\Delta E = E_f - E_i$, and $\Delta'\mu = 2\mu_{Cs} - \mu_{Cw}$, the chemical potentials. β is the inverse of the product of the temperature and the Boltzmann constant. In all simulations, the μ_{Cw} is set at -100 kCal/mol. 2500 Monte Carlo moves are attempted to equilibrate the system at 300 K and 0 Pa and 150 moves are attempted to measure the equilibrium concentrations of Cs and Cw.

In order to ensure that the potential energy minima captured the relevant thermodynamics, the procedure described above was modified, where structural relaxations were replaced by full molecular dynamics equilibration and sampling runs. $E_{\text{after}} - E_{\text{before}}$ was defined as the MD-generated free energy difference (using the free energy perturbation formalism). This modification did not lead to a significant change in the calculated sorption isotherms.

The C-S-H nanopore surface was considered as a sink and source of ions. While, exchange of Ca^{2+} for Cs^{1+} in the interlayer has a large effect on the substrate structure and energetics, given its highly constrained nature, exchange of ions at the surface has small effects on the substrate structure and energetics. Thus, the chemical potentials can be estimated by calculating the binding energies of Ca^{2+}. 2 to 20 Cs atoms are inserted in the nanopore. These correspond to concentrations of 0.02 to 0.2 Mol/L, which is on the high end of typical concentrations observed experimentally. To conserve the total charge, a Ca^{2+} is swapped for Cs^{1+} a second Cs^{1+} is inserted, in order to conserve the total charge of the system. In each case, a 1 ns NVT run and a 1 ns NPT run are performed to relax the system. The site potential energies are measured by averaging over 101 MD-generated configurations each separated by 1 ps.

D. Diffusion of Cs in C-S-H

The semi-grand-canonical procedure provides information about equilibrium uptake of Cs in cement paste but not about

equilibration timescales. The diffusion of Cs in the C-S-H grain is a limiting factor. The ion must find a pathway starting at the surface and diffuse through the interlayer. In principle, the diffusivity of Cs ions in C-S-H can be extracted from MD runs. However, our longest simulations—2 ns—led to Cs diffusion of a few Å. In other words, the Cs ions are trapped in local minima and jumps from one minimum to another are rare events. We solve this multiple timescale problem using transition-state theory. The energy difference ΔE_p between the potential energy minima and the saddle points ΔE_p gives the escape time out of a basin:

$$\tau = \tau_0 e^{\beta \Delta E_p}, \tag{3}$$

where τ_0 is a prefactor inversely proportional to an attempt frequency ν_0. β is the inverse of the product of the temperature and the Boltzmann constant. In order to identify the minima and saddle-points, single-ended saddle-point searches are performed; specifically, the activation relaxation technique *nouveau* (ARTn) [41–44] is chosen. Starting from a potential energy minimum, ARTn is able to autonomously sample the transition states connected to this minimum. ARTn has successfully been used to study diffusion and complex structural relaxation in metals [45,46], alloys [47,47], semiconductors [48–50] and amorphous solids [51]. An energy landscape exploration strategy is followed, where 1500 events with a global barrier—relative to the global minimum—smaller than a threshold are accepted. The maximum global displacement of Cs^+ ions in each 1500-event trajectory is calculated. τ_0 for each transition state is determined using the Vineyard equation [52]. A value of 1.5 THz is obtained. This value is lower than the standard 10 THz prefactor. This is mainly explained by the large mass of Cs.

During ARTn searches, displacements were allowed on all atoms in the system, but the initial random deformations were centered on Cs ions. This means that trajectories involving elaborate reorganization of atoms far away from the Cs ions were ignored. As a consequence, the diffusion times calculated in our study are an effective upper bound, as some faster pathways involving these reorganizations may not have been explored.

(1) The system is minimized to a local potential energy minimum E_{LM}.

(2) If $E_{\mathrm{LM}} < E_{\mathrm{GM}}$, set $E_{\mathrm{GM}} = E_{\mathrm{LM}}$ (E_{GM} is the current estimate of the system's global minimum potential energy).

(3) Generate an event using ARTn with saddle point energy E_{SP}.

(4) If $E_{\mathrm{SP}} - E_{\mathrm{GM}} < E_{\mathrm{threshold}}$, accept the event. Otherwise, reject it.

Using this procedure, a trajectory is generated with an overall barrier lower than a set threshold. Inspection of Eq. (1)—in the main paper—indicates that this corresponds to an overall upper bound on a waiting time.

E. Effect on mechanical properties (nano- and mesoscale)

The effects of Cs exchange with hydrated Ca in the interlayer on the mechanical properties of individual C-S-H grains are investigated. After MD relaxation, the bulk and shear moduli are calculated at 0 K. Volume expansion is measured at 300 K.

Since mesoscopic mechanical properties of C-S-H arise from grain-grain interactions, a multiple length-scale approach is needed to properly assess the effects of Cs^+ sorption. Two effects, (1) the volume expansion of C-S-H grains and (2) the concentration of Cs^+ in the pores of cement are considered by (1) increasing the particle size by 0.2 to 5% and (2) by evaluating the potential of mean force (pmf) between C-S-H grains in the presence of Cs^+.

Ioannidou's *et al.* mesoscale C-S-H model [53,54] was used to calculate the mesoscale expansive pressure generated by single C-S-H grain swelling, due to Cs adsorption in the interlayer. This length of the cubic simulation box is 390.36 nm, containing 177 975 particles. The interactions are modeled using Lennard-Jones (24/12) interaction potentials, calibrated to data from atomistic simulations and experiments [53,55]. These models capture structural and mechanical heterogeneities, emerging from the precipitation of C-S-H grains in confined space, and they reproduce a number of experimental properties such as pore size distributions and elastic moduli [54,55]. In order to calculate the residual stress due to swelling, all particle radii are inflated by the specified amount instantaneously from the original quenched configuration. After a first minimization to relax the large contact forces as a result of instantaneous swelling, MD relaxation of 25 000 steps at room temperature ($T = 0.00015$ in reduced units) are performed for each inflated configuration. These configurations are then relaxed by energy minimization using the conjugate gradient algorithm. Then the residual pressures are measured with respect to the original eigenstress before swelling. It is likely that Cs adsorption would be more important in C-S-H grains close to the pore network of cement. These grains can be identified via their packing fraction. Grains with their coordination numbers in the lowest 10% quantile are considered to neighbor a pore. Simulations where only those grains are inflated were performed. This reduces the overall expansive pressure in the system, compared to scenarios where all grains are expanded.

The simulations presented here suggest that, on average, Cs preferentially adsorbs in the C-S-H interlayer at the concentrations of interest for nuclear waste repository, at equilibrium. Nonetheless, it is probable that a fraction of the Cs may be present at the pore solution of cement paste, either because the system is out of equilibrium or because of local heterogeneities. This Cs at the pore solution in the gel pores will influence the potential of mean force (pmf) between C-S-H grains [56]. The effect of Cs concentration on these interactions was estimated using the so-called primitive model [57,58]. The surface charge was set at 0.02 e/Å^2. A total of 81 Ca^{2+} ions were initially added to the system. Then a fraction of the Ca^{2+} was replaced by Cs. Hydrated Ca^{2+} and Cs^+ radii were set at 3.0 Å and 2.5 Å, respectively. Relative permittivity was set at 10.

III. RESULTS

A. Sorption of Cs in C-S-H

In Figs. 2 and 3, the site binding energies of the Cs^+ and hydrated Ca^{2+} ions are reported. In the C-S-H interlayer, higher Cs^+ concentrations lead to larger Cs^+ site energies and to smaller Ca^{2+} site energies. At the nanopore surface, trends

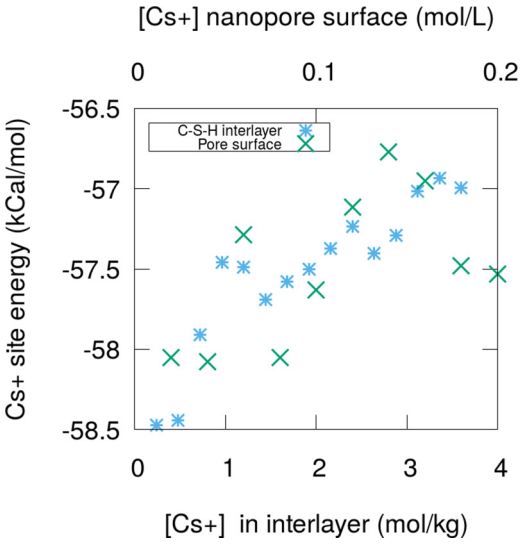

FIG. 2. The average site binding energies of Cs^+ in the C-S-H interlayer and at the nanopore surface.

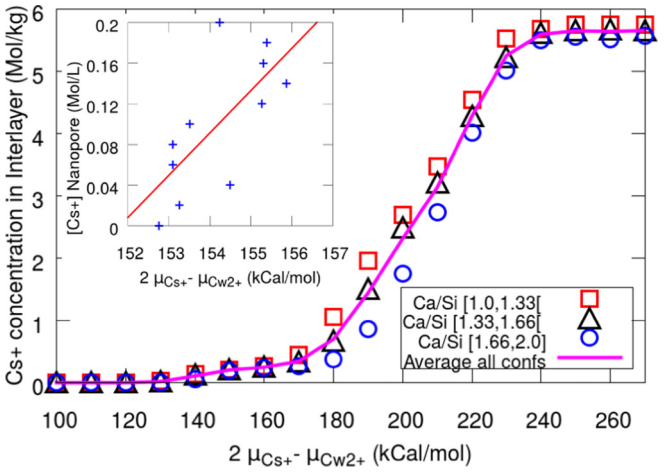

FIG. 4. Exchange isotherms of Cs and Ca in C-S-H interlayer—300 K. Each symbol corresponds to an average over configurations with similar Ca/Si ratios before Cs uptake. Inset: chemical potential estimated by averaging binding energies of ions at a C-S-H nanopore surface.

are less systematic, although it is observed that higher Cs^+ concentrations lead to larger Cs^+ site energies and to stable Ca^{2+} site energies.

The exchange isotherms in the C-S-H interlayer are plotted in Fig. 4. Each point represents an average over C-S-H configurations with a similar Ca/Si ratio before Cs uptake. Three features are observed. First, each set reveals a threshold potential, situated between $\Delta\mu' = 2\mu_{Cs+} - \mu_{Ca2+} = [120,140]$ kCal/mol. Second, as $\Delta\mu'$ further increases, the proportion of Cs in C-S-H increases and saturates as $\Delta\mu'$ nears 220 kCal/mol. Third, as the Ca/Si ratio of the initial C-S-H structure is increased, the $\Delta\mu'$ necessary to reach a given Cs uptake increases. The chemical potentials estimated at the nanopore surface are plotted in the inset of Fig. 4. The threshold potential is at $\Delta\mu' = 152.8$ kCal/mol, and the maximum nanopore uptake considered here is achieved at $\Delta\mu' = 161.1$ kCal/mol. These calculations indicate that Cs^+ adsorption happens preferentially in the interlayer until interlayer concentration reaches 0.19 Mol/kg and preferentially happens at the nanopore surface at higher concentrations.

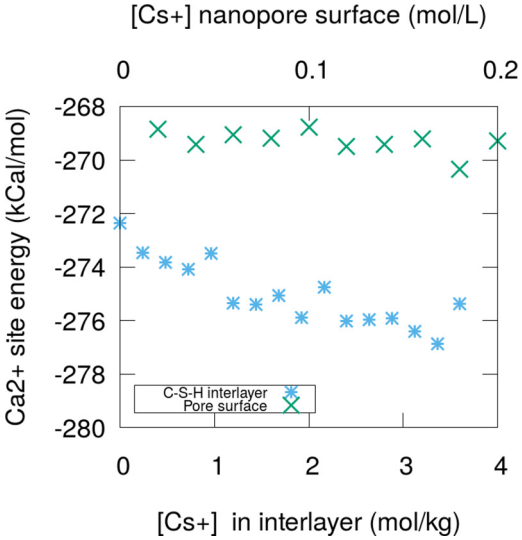

FIG. 3. The average site binding energies of Ca^{2+} in the C-S-H interlayer and at the nanopore surface.

B. Diffusion of Cs in C-S-H

The results for diffusion of Cs in C-S-H are presented in Fig. 5. Two main features are observed. First, there is an important variability of Cs diffusion from one sample to another. In some cases, Cs displacements were limited to a few Angstroms and reached up to 3 nm in other cases. No clear dependence of Cs displacements on C-S-H composition was observed. Second, the overall Cs displacements decrease as the activation barrier threshold is decreased. Cesium displacements as large as 1 nm are observed in simulation involving 23.06 kCal/mol or less. If one considers 1 nm as a minimal threshold for

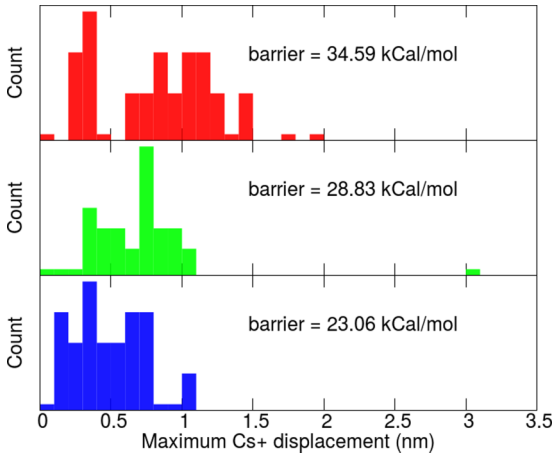

FIG. 5. The maximum Cs displacement observed in ARTn runs in C-S-H. These runs are set to accept ARTn events with an overall activation barrier lower than a preset threshold and reject those with a higher activation barrier.

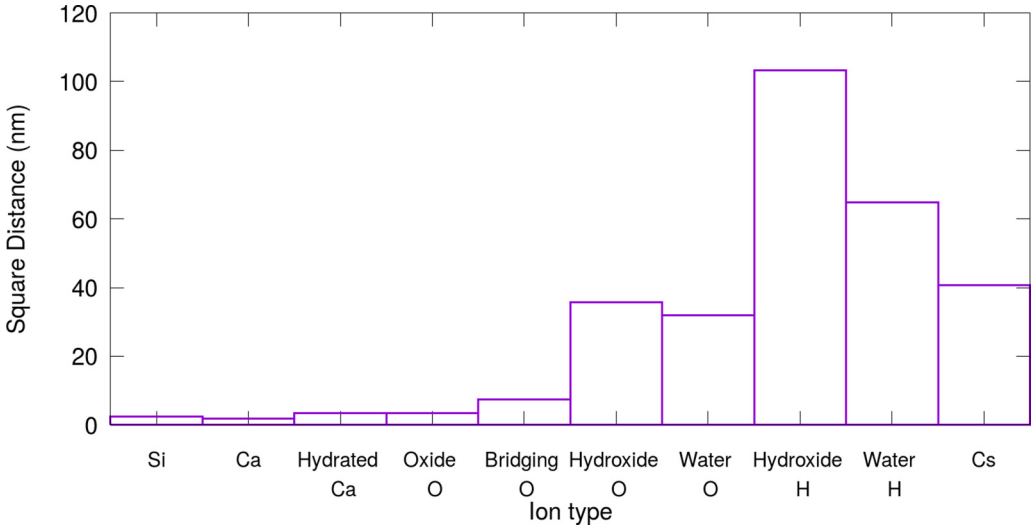

FIG. 6. Total squared displacement of each atomic specie over all the ARTn runs. It can be seen that Cs diffusion is mostly accommodated by water and hydroxide reorganization and that atoms in the oxide layers are displaced by small quantities.

diffusion, it implies a barrier of 23.06 kCal/mol as a lower bound for Cs diffusion. No clear trend is observed between Ca/Si ratios and Cs diffusion.

The overall activation energy for Cs can be estimated by subtracting the difference in site energy of Cs atoms on the pore surface and within the interlayer (1 kCal/mol, according to our calculations) from the bulk activation barrier, for an overall activation barrier of 22.06 kCal/mol. The characteristic time for each Cs jump during sorption is thus of the order of two hours at room temperature. Since sorption involves a few tens of these jumps, the overall characteristic sorption time is of the order of a few days. This computational result is consistent with the experimental results of Pointeau, and Li and Pang [15,18], which found a sorption time of about one day.

In Fig. 6, the total square displacement of all atoms, summed over all the ARTn runs, is plotted. Cs, water, and hydroxide molecules exhibit much larger squared displacements than the atoms forming oxide layers. In Fig. 7, the position of the Cs atoms, perpendicular to the C-S-H basal plane, is plotted. Each point represents one ARTn step. In two of the simulations, the Cs atom was initially placed in the oxide plane. It rapidly diffused out to the hydrated interlayer. Cs diffuses exclusively through the hydrated interlayers and never through the oxide—tobemorite-type—planes. The vast majority of Cs displacement is accommodated by displacements of water and hydroxides groups, while Ca (both in the oxide and the hydrated interlayers) and Si displacements are very limited.

C. Presence of Cs in the pore solution: Effect on intergranular binding

The results are plotted in Fig. 8. If one replaces 10% of the Ca^{2+} by Cs^{+}, the qualitative shape of the potential of mean force is preserved, but the binding energy is reduced by 6.5%. The effect of such a reduction in effective interaction between C-S-H grains in conjunction with grain swelling was investigated via the mesoscale model, as described in the

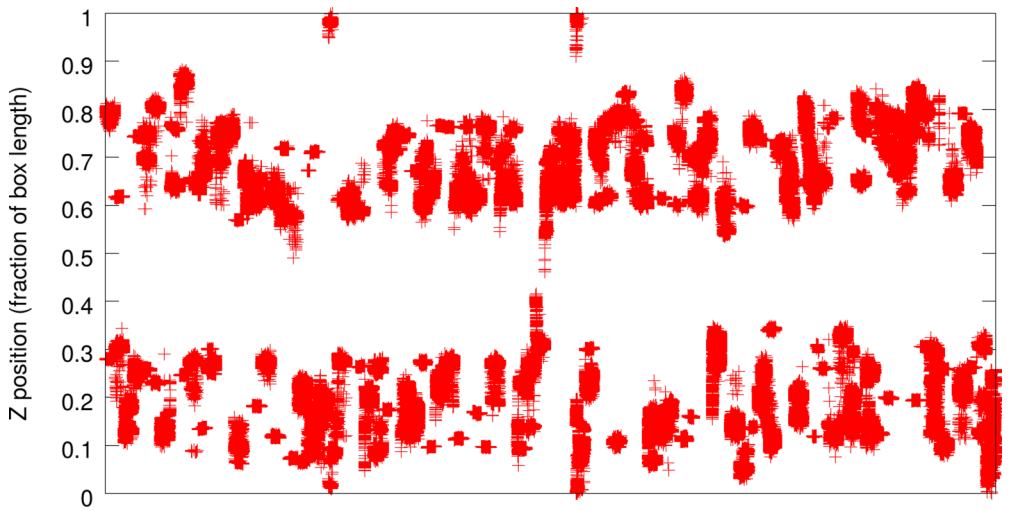

FIG. 7. The Z coordinates of Cs atoms in all the ARTn runs. The Z direction is perpendicular to the basal plane of C-S-H. The gap between the Cs positions correspond to the oxide—tobermorite-type—planes.

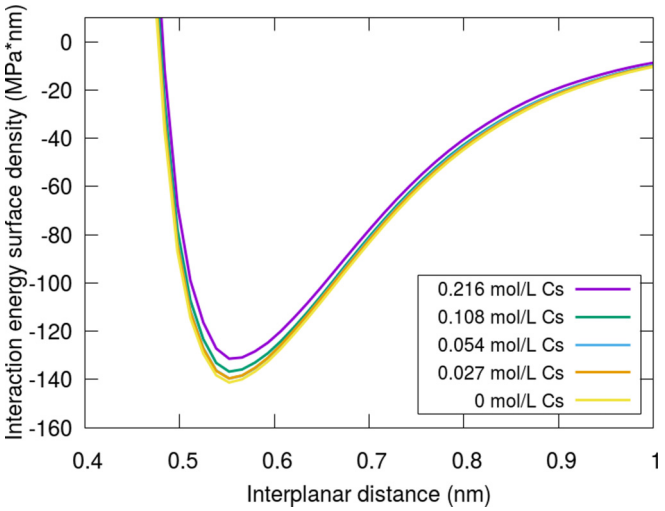

FIG. 8. Potential of mean force of two C-S-H grains with a 0.02 e/Å^2 surface charge. Calculations are done using the so-called primitive model. As cesium replaces calcium is introduced in the system, the depth of the free energy well decreases.

methodology and in the following section. The general effect of this reduction in the magnitude of the attractive energy well is to reduce the overall expansive pressure created by grain swelling.

D. Effect on mechanical properties

The effects of Cs exchange with hydrated Ca in the interlayer on the mechanical properties of individual C-S-H grains are investigated (Fig. 9). After MD relaxation, the bulk and shear moduli are calculated at 0 K. Volume expansion is measured at 300 K.

Figure 4(a) shows significant volume expansion that increases linearly with Cs uptake. This is consistent with changes in the basal distances measured by x-ray diffraction after exposure of C-S-H to CsCl and CsOH [9]. In Fig. 4(b), the bulk modulus decreases at Cs concentrations larger than 1 mol/kg. The Cs uptake does not have a systematic effect on the shear modulus of C-S-H as shown in Fig. 4(c). The change in mechanical properties, for a given Cs uptake, has a weak dependence on the Ca/Si ratio (more details in the Supplemental Material [30]).

Figure 4(d) shows the expansive mesoscale pressure of cement paste in four scenarios. Considering the presence of Cs^+ in the pore solution or limiting adsorption to grains near the pore reduces the expansive pressure. In typical repository conditions—Cs^+ concentrations well below 0.1 mol/kg—all mesoscale expansive pressures evaluated are of the order of 0–4 MPa, well within the elastic regime of C-S-H.

IV. DISCUSSION AND CONCLUSIONS

The nanoscale models suggests that interlayer adsorption of Cs in C-S-H significantly contributes to overall Cs sorption. These sites are generally preferred over nanopore surface sites at the concentrations of interest for repositories. C-S-H with low Ca/Si ratios generally sorb more Cs than C-S-H with high

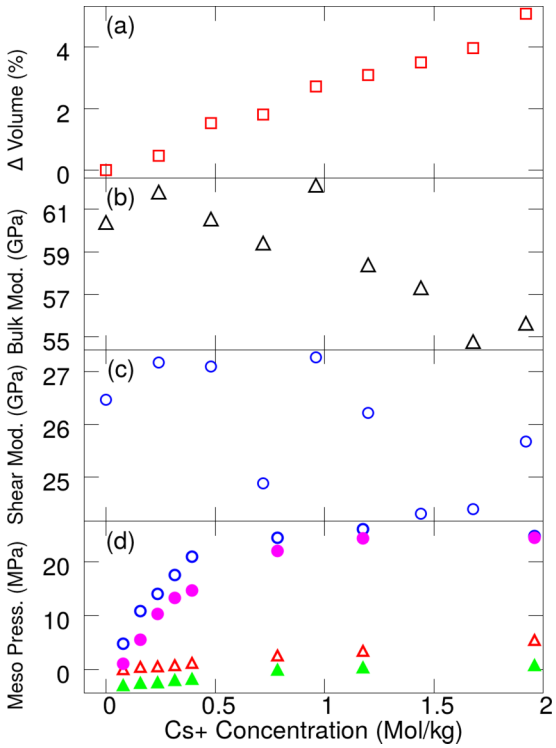

FIG. 9. Individual C-S-H grains: Effect on (a) volume change, (b) bulk modulus, and (c) shear modulus due to exchange of Ca and Cs ions in C-S-H interlayer. (d) Effect on the mesoscale assembly of grains: Triangles are scenarios where Cs was only adsorbed by grains neighboring pores, and circles are scenarios where Cs was adsorbed by all grains. Full (empty) symbols are scenarios with grain-grain interactions in the presence (absence) of Cs in the pore solution.

Ca/Si ratios, in accordance with Refs. [7,11,14,15], but in contradiction to Ref. [16]. Even though structures with high Ca/Si are more amorphous, electrostatic considerations favor sorption in C-S-H with low Ca/Si. These findings are valid within the limits of the C-S-H structural models and force fields used in this study.

Our calculations suggest that concentrations of Cs in the C-S-H grain reach equilibrium in a day or so at room temperature, which validates typical experimental protocols. It should be noted that the activation barriers calculated here are well below those found in Refs. [20,21]. As explained in Ref. [20], these barriers are much too high to account for experimentally observed diffusion. In fact, using a similar protocol used in these studies—using the NEB method—we found similarly large barriers. The ARTn generated trajectories with lower overall barriers than the NEB. Inspection of the ARTn trajectories suggests that water and hydroxide molecules are reconfigured during concerted activated events, involving small displacements of hydrated Ca ions. These reconfigurations facilitate the diffusion of Cs ions, notably by providing them more effective electrostatic screening. More generally, these calculations are a proof of principle that open-ended saddle-search methods—such as ARTn—can be used to generate physically realistic trajectories in C-S-H over experimental timescales.

Interestingly, the attempt frequency is close to the standard prefactor—10 THz—once accounting for the large mass of Cs. Likewise, our semigrand canonical Monte Carlo results indicate that the system is largely driven by its potential energy landscape. This justifies the use of a saddle-search method based on the exploration of the potential energy surface. This may come as a surprise, given the complexity of the C-S-H interlayer. Finally, it should be noted that this study ignored the contributions of quantum effects, such as zero-point motion and tunneling. Given the abundance of hydrogen in the model, these effects could be substantial.

The numerical model suggests that C-S-H is stable after insertion of Cs in its interlayer, and that its mechanical properties are largely preserved. Nanoscale grain expansion is to be expected by Cs uptake, but this leads to relatively little mesoscale expansive pressure.

The tobermorite-type planes in our models do not fragment when exposed to Cs. This contradicts the observations reported in Ref. [9]. These experimental results may be caused by drying the samples before characterization. Moreover, the Ca/Si ratios used in Ref. [9] are lower than 1.0, while the models presented here have Ca/Si ratios greater than 1.0. Finally, it is possible that our model failed to capture this phenomenon because of the limitations of CSH-FF.

Cs-137 beta radiation interaction with C-S-H was ignored in this study, since the CSH-FF potential cannot treat the ensuing physical chemistry. It leads to significant hydrolysis [59], in cement pores and—to a lesser extent—in the interlayer, which could affect mechanical, chemical, and transport properties of the paste. The methods presented here, including semigrand canonical Monte Carlo, ARTn, and mesoscopic models could be coupled to electronic structure calculations to further characterize the properties of C-S-H grains under such irradiation.

ACKNOWLEDGMENTS

This work was supported by the C-S-Hub at MIT and both the ICoME2 Labex (ANR-11-LABX-0053) and the A*MIDEX projects (ANR-11-IDEX-0001-02) cofunded by the French program "Investissements d'avenir," which is managed by the ANR, the French National Research Agency. L.K.B. acknowledges additional support from a fellowship awarded by the Natural Sciences and Engineering Research Council of Canada.

[1] A. Braun, D. Evans, P. M. Gandhi, M. Garamszeghy, H. Geiser, E. W. Hooper, F. D. Kaufmann, P. Luycx, B. Martynoy, L. J. Mezga *et al.*, *Application of Ion Exchange Processes for the Treatment of Radioactive Waste and Management of Spent Ion Exchangers* (International Atomic Energy Agency, Vienna, 2002).

[2] A. F. Holleman, *Holleman-Wiberg Inorganic Chemistry* (Academic Press, San Diego, 2001).

[3] M. P Unterweger, D. D. Hoppes, and F. J. Schima, New and revised half-life measurements results, Nucl. Instrum. Methods Phys. Res., Sect. A **312**, 349 (1992).

[4] H. Metivier, *Chernobyl: Assessment of Radiological and Health Impacts* (OECD, Paris, 2002).

[5] R. L. Bunting, Nuclear data sheets for A= 137, Nucl. Data Sheets **15**, 335 (1975).

[6] D. K. Gupta and C. Walther, *Impact of Cesium on Plants and the Environment* (Springer, Cham, 2017).

[7] N. D. M. Evans, Binding mechanisms of radionuclides to cement, Cement and Concrete Research **38**, 543 (2008).

[8] H. Viallis, P. Faucon, J.-C. Petit, and A. Nonat, Interaction between salts (nacl, cscl) and calcium silicate hydrates (c- s-h), J. Phys. Chem. B **103**, 5212 (1999).

[9] T. Iwaida, S. Nagasaki, S. Tanaka, T. Yaita, and S. Tachimori, Structure alteration of csh (calcium silicate hydrated phases) caused by sorption of caesium, Radiochimica Acta **90**, 677 (2002).

[10] E. Wieland, J. Tits, and M. H. Bradbury, The potential effect of cementitious colloids on radionuclide mobilisation in a repository for radioactive waste, Applied Geochemistry **19**, 119 (2004).

[11] M. Ochs, I. Pointeau, and E. Giffaut, Caesium sorption by hydrated cement as a function of degradation state: Experiments and modelling, Waste Management **26**, 725 (2006).

[12] S. Höglund, L. Eliasson, B. Allard, K. Andersson, and B. Torstenfelt, Sorption of some fission products and actinides in concrete systems, MRS Proc. **50**, 683 (1985).

[13] S. Bagosi and L. J. Csetényi, Caesium immobilisation in hydrated calcium-silicate-aluminate systems, Cem. Concr. Res. **28**, 1753 (1998).

[14] S. Bagosi and L. J. Csetenyi, Caesium immobilisation in hydrated calcium-silicate-aluminate systems, Cem. Concr. Res. **28**, 1753 (1998).

[15] I. Pointeau, Etude mecanistique et modelisation de la retention de radionucleides par les phases de silicate de calcium des ciments hydrates, Ph.D. thesis, These de l'Universite de Reims-Champagne-Ardennes, France (2000).

[16] S. Aggarwal, M. J. Angus, and J. Ketchen, Sorption of radionuclides onto specific mineral phases present in repository cements, Report AEA Technology NSS **312**, 1 (2000).

[17] S. Hoyle and M. W. Grutzeck, Effects of phase composition on the cesium leachability of cement-based waste forms, Waste Management **86**, 491 (1986).

[18] K. Li and X. Pang, Sorption of radionuclides by cement-based barrier materials, Cem. Concr. Res. **65**, 52 (2014).

[19] L. Dezerald, J. J. Kohanoff, A. A. Correa, A. Caro, R. J.-M. Pellenq, F. J. Ulm, and A. Saúl, Cement as a waste form for nuclear fission products: The case of 90sr and its daughters, Environ. Sci. Technol. **49**, 13676 (2015).

[20] L. Ruiz Pestana, K. Kolluri, T. Head-Gordon, and L. N. Lammers, Direct exchange mechanism for interlayer ions in non-swelling clays, Environ. Sci. Technol. **51**, 393 (2016).

[21] V. O. Ozçelik and C. E. White, Nanoscale charge-balancing mechanism in alkali-substituted calcium–silicate–hydrate gels, J. Phys. Chem. Lett. **7**, 5266 (2016).

[22] J. Jiang, P. Wang, and D. Hou, The mechanism of cesium ions immobilization in the nanometer channel of calcium silicate

hydrate: a molecular dynamics study, Phys. Chem. Chem. Phys. **19**, 27974 (2017).

[23] R. Shahsavari, R. J.-M. Pellenq, and F.-J. Ulm, Empirical force fields for complex hydrated calcio-silicate layered materials, Phys. Chem. Chem. Phys. **13**, 1002 (2011).

[24] R. T. Cygan, J.-J. Liang, and A. G. Kalinichev, Molecular models of hydroxide, oxyhydroxide, and clay phases and the development of a general force field, J. Phys. Chem. B **108**, 1255 (2004).

[25] P. A. Bonnaud, Q. Ji, B. Coasne, R. J.-M. Pellenq, and K. J. Van Vliet, Thermodynamics of water confined in porous calcium-silicate-hydrates, Langmuir **28**, 11422 (2012).

[26] M. J. A. Qomi, K. J. Krakowiak, M. Bauchy, K. L. Stewart, R. Shahsavari, D. Jagannathan, D. B. Brommer, A. Baronnet, M. J. Buehler, S. Yip *et al.*, Combinatorial molecular optimization of cement hydrates, Nat. Commun. **5**, 4960 (2014).

[27] R. X. Fischer and E. Tillmanns, Revised data for combeite, na2ca2si3o9, Acta Crystallogr., Sect. C: Cryst. Struct. Commun. **43**, 1852 (1987).

[28] R. C. Rouse, D. R. Peacor, and P. J. Dunn, Hydroxyapophyllite, a new mineral, and a redefinition of the apophyllite group; ii, crystal structure, Am. Mineral. **63**, 199 (1978).

[29] Y. A. Uvarova, E. Sokolova, F. C. Hawthorne, A. A. Agakhanov, L. A. Pautov, and V. Y. Karpenko, The crystal chemistry of senkevichite, cs k na ca 2 ti o [si 7 o 18 (oh)], from the dara-i-pioz alkaline massif, northern tajikistan, Can. Mineral. **44**, 1341 (2006).

[30] See Supplemental Material at http://link.aps.org/supplemental/10.1103/PhysRevMaterials.2.053608 for information about validation of interatomic potential and details of mechanical properties. .

[31] S. Plimpton, Fast parallel algorithms for short-range molecular dynamics, J. Comput. Phys. **117**, 1 (1995).

[32] M. Bauchy, M. J. A. Qomi, F.-J. Ulm, and R. J.-M. Pellenq, Order and disorder in calcium–silicate–hydrate, J. Chem. Phys. **140**, 214503 (2014).

[33] M. Bauchy, H. Laubie, M. J. A. Qomi, C. G. Hoover, F.-J. Ulm, and R. J.-M. Pellenq, Fracture toughness of calcium–silicate–hydrate from molecular dynamics simulations, J. Non-Cryst. Solids **419**, 58 (2015).

[34] M. J. A. Qomi, F.-J. Ulm, and R. J.-M. Pellenq, Physical origins of thermal properties of cement paste, Phys. Rev. Appl. **3**, 064010 (2015).

[35] A. Kumar, B. J. Walder, A. Kunhi Mohamed, A. Hofstetter, B. Srinivasan, A. J. Rossini, K. Scrivener, L. Emsley, and P. Bowen, The atomic-level structure of cementitious calcium silicate hydrate, J. Phys. Chem. C **121**, 17188 (2017).

[36] G. Kovačević, B. Persson, L. Nicoleau, A. Nonat, and V. Veryazov, Atomistic modeling of crystal structure of ca1. 67sihx, Cem. Concr. Res. **67**, 197 (2015).

[37] G. Kovačević, L. Nicoleau, A. Nonat, and V. Veryazov, Revised atomistic models of the crystal structure of c–s–h with high c/s ratio, Z. Phys. Chem. **230**, 1411 (2016).

[38] E. Pustovgar, R. P. Sangodkar, A. S. Andreev, M. Palacios, B. F. Chmelka, R. J. Flatt, and J.-B. d'Espinose de Lacaillerie, Understanding silicate hydration from quantitative analyses of hydrating tricalcium silicates, Nat. Commun. **7**, 10952 (2016).

[39] X. Cong and R. J. Kirkpatrick, 29si mas nmr study of the structure of calcium silicate hydrate, Adv. Cem. Based Mater. **3**, 144 (1996).

[40] M. Jeffroy, A. Boutin, and A. H. Fuchs, Understanding the equilibrium ion exchange properties in faujasite zeolite from monte carlo simulations, J. Phys. Chem. B **115**, 15059 (2011).

[41] G. T. Barkema and N. Mousseau, Event-Nased Relaxation of Continuous Disordered Systems, Phys. Rev. Lett. **77**, 4358 (1996).

[42] R. Malek and N. Mousseau, Dynamics of lennard-jones clusters: A characterization of the activation-relaxation technique, Phys. Rev. E **62**, 7723 (2000).

[43] E. Machado-Charry, L. K. Béland, D. Caliste, L. Genovese, T. Deutsch, N. Mousseau, and P. Pochet, Optimized energy landscape exploration using the ab initio based activation-relaxation technique, J. Chem. Phys. **135**, 034102 (2011).

[44] N. Mousseau, L. K. Béland, P. Brommer, J.-F. Joly, F. El-Mellouhi, E. Machado-Charry, M.-C. Marinica, and P. Pochet, The activation-relaxation technique: Art nouveau and kinetic art, J. At., Mol., Opt. Phys. **2012**, 925278 (2012).

[45] P. Brommer, L. K. Béland, J.-F. Joly, and N. Mousseau, Understanding long-time vacancy aggregation in iron: A kinetic activation-relaxation technique study, Phys. Rev. B **90**, 134109 (2014).

[46] L. K. Béland, Y. N. Osetsky, R. E. Stoller, and H. Xu, Slow relaxation of cascade-induced defects in fe, Phys. Rev. B **91**, 054108 (2015).

[47] L. K. Béland, Y. N. Osetsky, R. E. Stoller, and H. Xu, Interstitial loop transformations in fecr, J. Alloys Compd. **640**, 219 (2015).

[48] L. K. Béland, Y. Anahory, D. Smeets, M. Guihard, P. Brommer, J.-F. Joly, J.-C. Pothier, L. J. Lewis, N. Mousseau, and F. Schiettekatte, Replenish and Relax: Explaining Logarithmic Annealing in Ion-Implanted c-Si, Phys. Rev. Lett. **111**, 105502 (2013).

[49] L. K. Béland and N. Mousseau, Long-time relaxation of ion-bombarded silicon studied with the kinetic activation-relaxation technique: Microscopic description of slow aging in a disordered system, Phys. Rev. B **88**, 214201 (2013).

[50] L. K. Béland, E. Machado-Charry, P. Pochet, and N. Mousseau, Strain effects and intermixing at the si surface: Importance of long-range elastic corrections in first-principles calculations, Phys. Rev. B **90**, 155302 (2014).

[51] J.-F. Joly, L. K. Béland, P. Brommer, and N. Mousseau, Contribution of vacancies to relaxation in amorphous materials: A kinetic activation-relaxation technique study, Phys. Rev. B **87**, 144204 (2013).

[52] G. H. Vineyard, Frequency factors and isotope effects in solid state rate processes, J. Phys. Chem. Solids **3**, 121 (1957).

[53] K. Ioannidou, E. D. Gado, F.-J. Ulm, and R. J.-M. Pellenq, Inhomogeneity in cement hydrates: Linking local packing to local pressure, Journal of Nanomechanics and Micromechanics **7**, 04017003 (2017).

[54] K. Ioannidou, K. J. Krakowiak, M. Bauchy, C. G. Hoover, E. Masoero, S. Yip, F.-J. Ulm, P. Levitz, R. J.-M. Pellenq, and E. Del Gado, Mesoscale texture of cement hydrates, Proc. Natl. Acad. Sci. U.S.A. **113**, 2029 (2016).

[55] K. Ioannidou, R. J.-M. Pellenq, and E. Del Gado, Controlling local packing and growth in calcium–silicate–hydrate gels, Soft Matter **10**, 1121 (2014).

[56] K. Ioannidou, B. Carrier, M. Vandamme, and R. Pellenq, The potential of mean force concept for bridging (length and time) scales in the modeling of complex porous materials, EPJ Web Conf. **140**, 01009 (2017).

[57] A. Delville and R. J.-M. Pellenq, Electrostatic attraction and/or repulsion between charged colloids: A (nvt) monte-carlo study, Mol. Simul. **24**, 1 (2000).

[58] R. J.-M. Pellenq and H. Van Damme, Why does concrete set?: The nature of cohesion forces in hardened cement-based materials, MRS Bull. **29**, 319 (2004).

[59] S. Le Caër, L. Dezerald, K. Boukari, M. Lainé, S. Taupin, R. M. Kavanagh, C. S. cN. Johnston, E. Foy, T. Charpentier, K. J. Krakowiak *et al.*, Production of h 2 by water radiolysis in cement paste under electron irradiation: A joint experimental and theoretical study, Cem. Concr. Res. **100**, 110 (2017).

Correction: The omission of a second affiliation for the first author has been set right. This change necessitated renumbering of the subsequent affiliations.